Anomalous circulation in July 2019 resulting in mass loss on the Greenland Ice Sheet

Richard I. Cullather[1,2], Lauren C. Andrews[1], Michael J. Croteau[3], Nicolo E. Digirolamo[4,5], Dorothy K. Hall[2,4], Young-Kwon Lim[1,6], Bryant D. Loomis[3], Christopher A. Shuman[4,7], and Sophie M.J. Nowicki[4]

[1]Global Modeling and Assimilation Office, National Aeronautics and Space Administration, Goddard Space Flight Center, Greenbelt, Maryland, USA, [2]Earth System Science Interdisciplinary Center, University of Maryland, College Park, Maryland, USA, [3]Geodesy and Geophysics Laboratory, National Aeronautics and Space Administration, Goddard Space Flight Center, Greenbelt, Maryland, USA, [4]Cryospheric Science Laboratory, National Aeronautics and Space Administration, Goddard Space Flight Center, Greenbelt, Maryland, USA, [5]Science Systems and Applications, Inc., Glenn Dale, Maryland, USA, [6]Universities Space Research Association, Goddard Earth Sciences Technology and Research, Columbia, Maryland, USA, [7]University of Maryland, Baltimore County, Baltimore, Maryland, USA

Key words: Melt event, Greenland Ice Sheet, mass loss, jet stream

Abstract. Current mass loss on the Greenland Ice Sheet (GrIS) includes a significant contribution from surface runoff. The circumstances associated with melt events are important for understanding the global sea level contribution of the GrIS. In late July 2019, surface melt occurred over 62 percent of the GrIS, including Summit Station. The general circulation leading to the event is found to be dissimilar to 2012 and other events documented in the 21st Century, with warm air associated with remote atmospheric blocking over western Europe eventually

transiting west to the GrIS. Gravimetric data indicate that the 2019 summer mass loss was 137 Gt more than the 2004-2010 median, or about 92 percent of the 2012 record. Mass loss during the event was significant in GrIS northeastern regions in 2019. As compared to 2012, the southwest did not fully participate. Similar circulation patterns have not previously been associated with significant melt.

1. Introduction

In recent assessments of global sea level, attention has focused on the contributions of polar ice sheets. Satellite altimetry, gravimetric data, and in situ observation assessments suggest that ice sheet mass loss continues to accelerate (e.g., Meredith et al., 2019). For the Greenland Ice Sheet (GrIS), about half of the current mass loss (50.3 percent) is attributable to a reduction in surface mass balance, owing to an increase in meltwater runoff (The IMBIE Team, 2019). The processes associated with surface mass loss have been extensively studied, particularly in light of recent melt events (e.g., van den Broeke et al., 2017; Hanna et al., 2013; Cullather et al., 2016; Mioduszewski et al., 2016; Trusel et al., 2018). The summer of 2012 saw widespread melt on the GrIS surface and significant mass loss (Tedesco et al., 2013; Hanna et al., 2014; Fausto et al., 2016), including 11- and 12-July when melt was simultaneously observed on nearly the entire GrIS (Hall et al., 2013). Melt and above-freezing air temperatures were observed at Summit Station (72°N, 38°W, 3216 m; hereafter “Summit”) on 11-July which, based on glaciological records, had occurred only once previously in the past 800 years (Nghiem et al., 2012). Other melt events have occurred at lower elevations since the turn of the century (Hanna et al., 2008; Steffen et al., 2004; Tedesco et al., 2008; Box et al., 2010). These events exhibit variability in their manner and duration. With rare exceptions for the northern basin (Tedesco et al., 2016),

they are persistently focused on the western margins (Graeter et al., 2018), which are located on the windward side of the ice sheet under typical atmospheric circulation patterns (Hanna et al., 2014).

Some examined factors that potentially drive melt events include: the role of various surface energy budget components, including (1) enhanced longwave radiative fluxes associated with warm, moist air intrusions and cloudiness (van Tricht et al., 2016; Bennartz et al., 2013; Cullather and Nowicki, 2018), (2) enhanced shortwave flux absorption associated with reduced cloudiness and ice surface darkening due to surface feedbacks, preconditioning through reduced winter or spring snow cover (Dyurgerov and Meier, 1999), or aerosol deposition (Box et al., 2012; Hofer et al., 2017; Tedesco et al., 2011; Thomas et al., 2017), or (3) changes in turbulent fluxes (Fausto et al., 2016); (4) the effects of reduced sea ice cover on eastward advecting warm and moist conditions (Rennermalm et al., 2009; Liu et al., 2016; Stroeve et al., 2017; Noël et al., 2014); and (5) various mechanisms of atmospheric circulation, including North Atlantic blocking, circulation trends over the Arctic Ocean (Lim et al., 2016; Hanna et al., 2013; Häkkinen et al., 2014; Tedesco et al., 2016), and extreme moisture transport (Neff, 2018; Mattingley et al., 2018). Local high-pressure blocking has been associated with surface melt events in 2002, 2003, 2007, 2010, and 2012 (Hanna et al., 2008; Nghiem et al., 2012). But prior analysis has suggested that local blocking is an endemic contributor to enhanced surface melt, including lesser events (e.g., Lim et al., 2016; Cullather and Nowicki, 2018; Rajewicz and Marshall, 2014; Hanna et al., 2016). The relation has led to the developed use of the Greenland Blocking Index (GBI; Hanna et al., 2014).

On 30- and 31-July 2019, widespread surface melt was observed across the GrIS, and above-freezing temperatures were again measured at the NOAA Summit automatic weather

station (AWS; Tedesco and Fettweis, 2019). Here, we employ atmospheric reanalyses (Modern-Era Retrospective analysis for Research and Applications, version 2: MERRA-2; Gelaro et al., 2017) and satellite observations from the Moderate-resolution Imaging Spectroradiometer (MODIS; Hall et al., 2018) and the Gravity Recovery and Climate Experiment (GRACE/GRACE-FO) to characterize daily circulation patterns in the week leading to the 2019 event, quantitatively describe the extent and duration of surface melt, examine the amount and spatial distribution of the associated GrIS mass loss, and provide context in relation to prior melt events in the 2003-2018 satellite data record. The analysis reveals a warm air mass previously associated with a western European heatwave was advected north and westward across the marginal seas of the North Atlantic. Ultimately, this event produced significant melt and mass loss along the northeastern side of the GrIS, and enhanced anticyclonic circulation patterns that drove mass loss elsewhere on the ice sheet.

2. Atmospheric Conditions

Figure 1(a) shows the evolving jet stream pattern associated with the melt event in late July and early August 2019. An omega blocking pattern – characterized by a high-amplitude ridge or northward distending area of high pressure in the upper troposphere and surrounded to its east and west by high-amplitude troughs – emerged over western Europe in the early part of the week of 21-July (Fig. 1(a)), producing northward, warm air advection from North Africa. By 24-July, the ridging pattern was centered over western Europe near 9°E, with a lee trough near 30°E and a strengthening windward trough over the central North Atlantic near 28°W. Within this long wave ridging pattern, a minor wave was embedded within the windward trough near the British Isles, which intensified the southerly flow along the western side of the ridge. The

blocking pattern resulted in record temperatures in several locations (Magnusson, 2019; Graham and Huggett, 2019). On 25-July, station data (Smith et al., 2011) for Paris-Montsouris, France reached 42°C while Brussels, Belgium and Cologne, Germany exceeded 36°C. On 26-July, reanalyses indicate the upwind trough of the blocking pattern became negatively tilted (Fig. 1(a)) as the ridge advanced northward to form a closed-circulation anticyclone over Scandinavia. A temperature of 32°C was reached at Bergen, Norway on 26-July and at Helsinki, Finland on 27-July. The negative tilt of the trough folded the jet stream into a southeast-to-northwest orientation over the North Atlantic, oriented from the British Isles to eastern Greenland. The surface warm air mass over Europe then followed the westward tilt of the jet stream onto the GrIS, initiating enhanced surface melt on 29-July.

A MODIS data-based analysis of aerosol concentrations (Randles et al., 2017) indicates a large transport from Europe over the North Sea on 26-July, with optical thicknesses of up to 0.1 (Supporting Information Fig. S1). The composition is recognized to be largely associated with Saharan dust. Over the subsequent two days, the analysis suggests a dispersal over the North Atlantic, with remaining amounts becoming topographically blocked upon nearing Greenland. For the time associated with the melt event, there is insufficient evidence of significant aerosol deposition on the ice sheet.

Rawinsonde data from Scoresbysund (71°N, 22°W, 70 m) for 12UTC 26-July to 29-July indicate an advancing warm layer with temperatures exceeding the prior week's conditions by 5-10°C throughout the troposphere, with an above-freezing layer extending from the surface to 700 hPa (Durre and Yin, 2008; Fig. 2c,d,e). It may be seen from the profiles that mid-tropospheric temperatures increased first, with values at Scoresbysund reaching 0°C at 730 hPa on 26-July. The warmest part of the profile is at 839 hPa on 27-July and 814 hPa on 28-July; a

near-surface inversion forms after 29-July. A similar downward progression occurred at Danmarkshavn (77°N, 19°W, 11 m), and is consistent with very slow warm air advection. Summit profiles also show a downward progression of temperature increases throughout the troposphere, with an increase of almost 10°C at 500 hPa by 30-July. After 29-July, the Summit profile indicates a near-surface inversion, with the surface pinned near the melting point on 30-July.

3. Surface melt and mass loss

Ice surface temperatures (IST), indicative of the surface melt/freeze state, were computed from available Terra swath observations from the Moderate-resolution Imaging Spectroradiometer (MODIS) for each 24-hr period between 25-July and 5-August (Hall et al., 2018). Daily melt extent is determined by applying an IST threshold selected, wherein melt is identified for locations where the IST is greater or equal to the threshold value. The value is based on the accuracy of the product and a long-term comparison with other observations (Adolph et al., 2018). The retrieval is only available for cloud-free conditions (Moeller et al., 2018).

Between 29-July and 1-August, MODIS IST observations indicate that between 21 and 52 percent of the GrIS experienced surface melt, with a peak observed extent occurring on 1-August as shown in Fig. 2a (see also Supporting Fig. S5). It may be seen from the figure that there is extensive cloud cover just prior and at the onset of the melt event, particularly on 29- and 30-July (covering 22 and 19 percent, respectively). This restricted the ability of MODIS to detect surface melting across the central and southern GrIS, including Summit. Basins shown in Fig. 1 (Zwally et al., 2012) are used to identify regions broadly homogeneous regarding surface slope

orientation relative to atmospheric advection. Here, cloud cover was particularly prevalent in basins 3 and 4. Nevertheless, MODIS IST data indicated substantial melt across the eastern and northern GrIS, with melt extent exceeding 80 percent of basin 2 on 30 and 31-July.

Reanalyses may contribute additional information on surface conditions where there is significant cloud cover. MERRA-2 has compared favorably with satellite observations of surface melt (Reeves Eyre and Zeng, 2017; Hall et al., 2018; Cullather et al., 2016), and is used for consistency with the identified general circulation. As noted in Hall et al. (2018), confidence in ice sheet surface properties increases when different datasets are used to produce a similar result. Between 29-July and 1-August, MERRA-2 indicated that between 30 and 62 percent of the ice sheet experienced surface melting (Fig. 2b; see Supporting Fig. S6). Peak melt extent was observed on 30-July, when 62 percent of the ice sheet – including Summit – experienced surface skin temperatures at or above 0°C. Surface melt was particularly widespread over central GrIS basins 3 (89 percent) and 7 (98 percent). There was also extensive surface melt on 31-July (61 percent), though MERRA-2 does not indicate melt at Summit, nor is widespread melt indicated over the central GrIS on this day. Rather, the reanalysis indicates extensive melt in northern basin 1 (greater than 78 percent) and in northeastern basin 2 (48 percent), as well as large parts of southwestern basins 5 and 6. MODIS data suggest the more extensive melt in the northern basins occurred on the prior day, 30-July. Nevertheless, the time-averaged surface melt extent pattern in MODIS and MERRA-2 are in general agreement (Fig. 2a,b); there are discrepancies in the southern GrIS, where extensive cloud cover during the initial phase of the melt event obscured MODIS retrievals.

Also shown in Fig. 2 is the Summit time series of observed air temperatures and corresponding values from reanalyses. Temperatures exceeded 0°C for 11.2 hr on 30-July, and

again for 5.5 hr on 31-July, reaching a maximum value of 1.2°C on the second day. The time series is remarkable, and is substantially longer than the historic 2012 event when the melting point was reached for 6.5 hours on one day (McGrath et al., 2013). Corresponding values from the reanalysis for 2019, which indicate some differences in the diurnal cycle but nevertheless approximate the day-to-day variability of the station measurements.

An examination of the surface energy budget finds a nuanced time series leading to the melt event. Though reanalysis representations of the GrIS surface energy budget can be problematic (e.g., Cullather et al., 2014), MERRA-2 has reasonably reproduced observed cloud radiative forcing and surface albedo (Wang et al., 2019). The energy budget evolution is also supported by the Scoresbysund AWS (Fig. 3). Reanalysis fields indicate the daily-averaged surface downwelling thermal flux increased markedly over basin 3 in the eastern GrIS prior to the melt event, while the solar flux decreased. From an average of 197 W m^{-2} on 24-July, the longwave flux increased by 80 W m^{-2} by 29-July (Fig. 3; see Supporting Fig. S10). From an average of 301 W m^{-2} on 24-July, the downwelling shortwave flux was lower by 109 W m^{-2} on 29 July. Over the ensuing two days, the downwelling longwave flux gradually decreased while the downwelling shortwave flux rapidly increased to pre-event levels. Relative to 29-July, the downwelling longwave flux was 7 W m^{-2} lower on 30-July and 28 W m^{-2} lower on 31-July, while the shortwave was higher by 61 W m^{-2} on 30-July, and by 88 W m^{-2} on 31-July. During this transitional period, the total downwelling radiative flux, the net surface radiative flux, and the surface air temperature were maxima for the examined period, and ice sheet surface melt became widespread. Turbulent fluxes added an additional 18 W m^{-2} during this period, or 41 percent of the net surface flux. Cloud masking from the MODIS temperature data support the

east-to-west passage of a cloud shield over 26 to 29-July, prior to the arrival of warmest surface temperatures on the eastern GrIS (see Supporting Fig. S4).

Reanalysis and GRACE/GRACE-FO data are used to characterize mass loss changes associated with this melt event. While MERRA-2 surface runoff has compared favorably with observations (e.g., Smith et al., 2017), the surface representation is of intermediate complexity and has no explicit firn representation (Cullather et al., 2016).

Reanalysis fields suggest that surface runoff increased markedly from 28-July to 2-August, with the largest amount occurring on 31-July of 1.42 Gt. Over this 6-day period, the total runoff was 6.4 Gt. This may be compared with the historic 2012 melt event (Supporting Table S1). Over the period 10-15 July of 2012, reanalyses indicate runoff of 7.7 Gt, suggesting the significance of the 2019 event. More intriguing is the breakdown of these amounts by basin. In the 2012 event, southwestern basin 6 accounted for largest fraction, nearly 29 percent of the total amount. In 2019, basin 6 only accounted for 19 percent, while northeastern basins 2 and 3 contributed 35 percent of the total. In comparing the 2012 and 2019 events, it is found that the northeastern basins provided similar amounts of runoff, while the southwestern basins provided about 44 percent less runoff in 2019 as compared with 2012.

Gravimetric solutions from GRACE/GRACE-FO are available at resolutions of 300-500 km and at monthly time scales (Loomis et al., 2020; see Supporting Information Fig. S7). Thus, changes over the June to August time period examined here may result from the ambient conditions and are not necessarily directly attributable to the melt event of 30-July to 1-August. The gravimetry observations are also not limited to surface changes but measure total mass variability. Surface melt may impact underlying glacier mass on a delayed time scale, from englacial and subglacial routing and retention (Nienow et al., 2017). These gravimetric observing

attributes are realized in comparing total mass loss with reanalysis surface estimates over the melt event, but are nevertheless of interest.

We compute basin-averaged mass loss from GRACE/GRACE-FO from the Univ. Texas at Austin's Center for Space Research (CSR) RL06 Level-2 spherical harmonics solution, using the averaging kernel method (Swenson and Wahr, 2002) and applying GRACE Technical Notes 13 and 14 to restore geocenter motion (Sun et al., 2016) and replace C_{20} and C_{30} values (Loomis et al., 2019, 2020). Effects due to glacial isostatic adjustment are removed using the ICE-6G_D (VM5a) model (Peltier et al., 2018).

Figure 4 presents mass loss anomalies relative to each year's maximum value for (a) the total GrIS, (b) northern GrIS, defined as Zwally basin 1, (c) eastern GrIS, defined as the sum of basins 2 and 3, and (d) southern GrIS, defined as the sum of basins 4, 5, and 6. By considering basin clusters, signal leakage errors associated with the limited spatial resolution of monthly GRACE products are mitigated. The reported 2-σ uncertainties include the solution noise, processing differences, and leakage errors. For the total GrIS, the August minus June monthly values indicate a late-summer loss of 420±142 Gt for 2019. This compares with losses of 459±140 Gt and 443±125 Gt for 2012 and 2016, respectively, and a mean loss of 283±99 Gt for the years 2004-2010 (shown in grey). Regionally, the 2019 June-to-August mass losses are 65±41 Gt, 114±79 Gt, and 147±73 Gt for northern, eastern, and southern GrIS, respectively. For 2012, losses of 43±48 Gt, 141±77 Gt, and 194±54 Gt are found for the same three regions. We note that the late summer losses in the northern GrIS (basin 1) are the largest of the GRACE/GRACE-FO record. Combining the northern and eastern regions results in comparable mass losses in 2012 and 2019, while losses in the southern region were a larger contributor in 2012 (42 percent of the total) than in 2019 (35 percent of the total). Consistent with reanalysis

output for the days encompassing the surface melt, gravimetric data indicate a significant event in 2019 that is somewhat smaller than in July 2012, and with a distinctly different pattern of mass loss.

4. Surface melt historical context

The circulation mechanisms leading to the 2019 melt event contrast with those associated with previous events in the satellite record (e.g., Häkkinen et al., 2014; Cullather and Nowicki, 2018) in several respects. Prior events are largely associated with transient blocking over the North Atlantic, leading to the redirection of subtropical warm air northward over the western GrIS. For example, Fig. 1(b) shows jet stream patterns for several significant melt events in which a high-pressure ridging pattern forms in close proximity to the ice sheet. In the melt event of 12 July 2012, for example, a mid-latitude blocking ridge formed near 35°W over several days, eventually extending north to the Denmark Strait and forming a heat dome over the ice sheet that was maintained for an extended period (Nghiem et al., 2012). Such North Atlantic blocking led to a nearly barotropic advection of warm, moist air onto the ice sheet. The 2019 pattern shown here actually coincides with low pressure over the North Atlantic (Fig. 1(d)), although the arrival of the warm air mass eventually resulted in anticyclonic circulation over much of the central and northern regions of the ice sheet. For 2019, the rapid folding of the jet stream resulted in a westward advection of warm air in the middle and upper troposphere that preceded surface warming. The advection is similar to that of a mid-latitude warm front, albeit at a greatly slowed rate due to the jet stream folding and planetary wave interaction at higher latitudes. This baroclinic temperature advection likely resulted in the phased response of surface energy budget components, which differs significantly from previous melt events.

A key aspect of the antecedent circulation is the bending of the jet stream towards the northwest. The streamline configuration of 26-July – oriented from southeast over the British Isles to northwest over the GrIS as contained within the dashed region shown in Fig. 1(a) – was compared with prior summer conditions (June, July, and August; JJA) in MERRA-2 over the satellite observing era using pattern correlation (see Supporting Fig. S11). Similar patterns are infrequent but not rare, occurring on average about once per year. An intriguing analogy occurred on 26-28 June 2003 during an extended European heatwave (Black et al., 2004). While the pattern shared characteristics with late July 2019, it did not fully extend westward to the GrIS, and any associated surface melt was largely unremarkable. Limiting factors for this mechanism are the longitudinal range of the jet excursion – which in the 2019 case extended from western Europe all the way to the ice sheet – and access to warm, subtropical air. An additional factor is the duration of the jet folding, which was sustained for several days in 2019 and allowed the warm air mass to traverse onto the ice sheet. Atmospheric heat and moisture transports parallel the jet stream during this event (Supporting Information Figs. S2-S4). The values are consistent with an extreme atmospheric moisture transport event (Liu and Barnes, 2015; Mattingley et al., 2018), but again differ in location and orientation to previous melt events examined.

A potential factor in the 2019 event is ice surface preconditioning. Tedesco and Fettweis (2019) note that the 2019 melt season began early, reducing the snowpack. The summer period was characterized by an unusually persistent anticyclone over the GrIS, with a melt event between 11-17 June. Passive microwave results of Tedesco and Fettweis (2019) and reanalyses suggest that almost half of the ice sheet experienced melt on 13-June (see Supporting

Information Fig. S6), potentially leading to decreased surface albedo and snowpack warming, which can result enhanced feedback mechanisms later in the season.

Persistent high pressure over the ice sheet, as indicated with the GBI, has been associated with reduced cloud cover and enhanced solar radiation, although recent work has also found an association with the northward advection of warm, moist air along the western margins of the ice sheet (Neff et al., 2014). During the late July 2019 event, high pressure likely provided subsidence which allowed warmer air to more rapidly mix downward to the surface. The circulation for this event was confined to the central and northern regions of the GrIS and largely excluded the southwestern margins from the direct influence of advecting warm air (e.g., Fig. 1(d)).

Indices of atmospheric teleconnections are also examined to assess whether the prevailing summertime general circulation was conducive to a melt event. Similar to the GBI, these indices are more associated with central North Atlantic blocking, rather than westward advection indicated for the 2019 event. Studies have shown the negative phase of the North Atlantic Oscillation (NAO) is more conducive to blocking (e.g., Fettweis et al., 2013; Hanna et al., 2015), while the positive phase of the East Atlantic (EA) pattern – the second principal model of North Atlantic variability (Trigo et al., 2008) – has also been correlated with enhanced GrIS summer warming (Lim et al., 2016). Principal component-based indices from the NOAA Climate Prediction Center for summer months (JJA) indicate that the NAO was in the negative phase for 2019, and that the index was the seventh lowest value of the 1950-2019 record. The EA index was also strongly positive for JJA, continuing a series of positive values over the last two decades. The JJA average of the GBI was also at a record level (a value of 5567). In this

context, these indices suggest sustained warmer conditions over the summer period which may have preconditioned the ice sheet surface.

5. Discussion

A review of the various factors examined in previous melt events highlights unique features of the late July 2019 conditions. The phased time series of surface radiative fluxes shown do not easily comport with prior determinations on the importance of longwave versus shortwave forcing. Rather, an increased net surface energy flux resulted from the interplay of downwelling flux components in the presence of an advancing cloud field. Anomalies in coastal sea ice cover are unlikely to have played a role in the 2019 event. In the vicinity of Scoresbysund, ice extent was only coastally proximal by late July, and was similar to recent years in the satellite era (e.g., Fetterer et al., 2017). The ice extent near Fram Strait and in Baffin Bay, which became ice-free in mid-July, was also unremarkable in comparison to recent years. While general circulation indices are consistent with previous melt events, the indexes are generally used to identify blocking over or very near the ice sheet, as opposed to the remote blocking that occurred here.

Prior to 2012, surface melt at Summit had occurred once in 800 years (Nghiem et al., 2012), but has now occurred twice in about 7 years. The infrequent nature of melt at Summit and the unusual manner of this event dissuades conclusions regarding trends. Nevertheless, these recent events are consistent with increasing surface melt found elsewhere on the GrIS (The IMBIE Team, 2019).

The large excursion of the jet stream is an intriguing aspect of this event. While some studies have suggested a tendency for low index flow in the presence of a warming climate, such

conclusions remain contentious (e.g., National Research Council, 2014; Gillett and Fyfe, 2013; Francis and Vavrus, 2012). In a warming climate, it is possible that the effects of infrequent circulation conditions on the GrIS are simply becoming more acute. It remains to be seen if a wider variety of anomalous circulation patterns may become associated with surface melt under these conditions.

Acknowledgments. MERRA-2 (Global Modeling and Assimilation Office, 2015a, 2015b) and MODIS ice surface temperature data were obtained from the Goddard Earth Sciences Data and Information Services Center. Rawinsonde data were obtained from the Integrated Global Rawinsonde Archive, NOAA National Centers for Environmental Information. Climate indices were obtained from the NOAA Climate Prediction Center. Automatic weather station data were obtained from the Programme for Monitoring of the Greenland Ice Sheet (https://promice.org/PromiceDataPortal/api/download/f24019f7-d586-4465-8181-d4965421e6eb). Summit temperatures were obtained from the NOAA Earth System Research Laboratory (https://www.esrl.noaa.gov/gmd/dv/site/index.php?stacode=SUM) by M. Schnaubelt, Univ. Maryland-Baltimore County. GRACE/GRACE-FO RL06 Level-2 spherical harmonic data and associated Technical Notes were obtained from Physical Oceanography Distributed Active Archive Center (PO.DAAC) at the Jet Propulsion Lab (https://podaac.jpl.nasa.gov/). The authors thank G.S. Partyka for useful discussions. This work was funded by the NASA Sea Level Change Team and the Modeling, Analysis, and Prediction programs. Michael Croteau's work was also supported by an appointment to the NASA Postdoctoral Program at Goddard Space Flight Center as administered by Universities Space Research Association.

References

Adolph, A.C., M.R. Albert, and D.K. Hall (2018). Near-surface temperature inversion during summer at Summit, Greenland, and its relation to MODIS-derived surface temperatures. *The Cryosphere*, **12**(3), 917-920. https://doi.org/ 10.5194/tc-12-907-2018

Bennartz, R., M.D. Shupe, D.D. Turner, V.P. Walden, K. Steffen, C.J. Cox, M.S. Kulie, N.B. Miller, and C. Pettersen (2013). July 2012 Greenland melt extent enhanced by low-level liquid clouds. *Nature*, **496**(7443), 83-86. https://doi.org/10.1038/nature12002

Black, E., M. Blackburn, G. Harrison, B. Hoskins, and J. Methven (2004). Factors contributing to the summer 2003 European heatwave. *Weather*, **59**(8), 217-223. https://doi.org/10.1256/wea.74.04

Box, J.E., J. Cappelen, D. Decker, X. Fettweis, T. Mote, M. Tedesco, and R.S.W. van de Wal (2010). Greenland. In J. Richter-Menge and J.E Overland (Eds.), *Arctic Report Card: Update for 2010* (pp. 55-64). https://doi.org/10.7916/D8XW4JQX

Box, J.E., X. Fettweis, J.C. Stroeve, M. Tedesco, D.K. Hall, and K. Steffen (2012). Greenland ice sheet albedo feedback. Thermodynamics and atmospheric drivers. *The Cryosphere*, **6**(4), 821-839. https://doi.org/10.5194/tc-6-821-2012

Cullather, R.I., and S.M.J. Nowicki (2018). Greenland Ice Sheet surface melt and its relation to daily atmospheric conditions. *J. Climate*, **31**(5), 1897-1919. https://doi.org/10.1175/JCLI-D-17-0447.1

Cullather, R.I., S.M.J. Nowicki, B. Zhao, and M.J. Suarez (2014). Evaluation of the surface representation of the Greenland Ice Sheet in a general circulation model. *J. Climate*, **27**(13), 4835-4856. https://doi.org/10.1175/JCLI-D-13-00635.1

Cullather, R.I. S.M.J. Nowicki, B. Zhao, and L.S. Koenig (2016). A characterization of Greenland Ice Sheet surface melt and runoff in contemporary reanalyses and a regional climate model. *Front. Earth Sci.*, **4**, 10. https://doi.org/10.3389/feart.2016.00010

Durre, I., and X. Yin (2008). Enhanced radiosonde data for studies of vertical structure. *Bull. Amer. Meteorol. Soc.*, **89**(9), 1257-1262.

Dyurgerov, M.B., and M.F. Meier (1999). Analysis of winter and summer glacier mass balances. *Geografiska Ann. Ser. A*, **81A**(4), 541-554. https://doi.org/10.1111/j.0435-3676.1999.00082.x

Fausto, R. S., van As, D., Box, J. E., Colgan, W., Langen, P. L., and Mottram, R. H. (2016). The implication of nonradiative energy fluxes dominating Greenland ice sheet exceptional ablation area surface melt in 2012. *Geophys. Res. Lett.*, **43**(6), 2649-2658. https://doi.org/10.1002/2016GL067720

Fetterer, F., K. Knowles, W.N. Meier, M. Savoie, and A.K. Windnagel (2017). Sea Ice Index, Version 3. Boulder, Colorado USA. NSIDC: National Snow and Ice Data Center. https://doi.org/10.7265/N5K072F8

Fettweis, X., E. Hanna, C. Lang, A. Bellefamme, M. Erpicum, and H. Gallée (2013). Important role of the mid-tropospheric atmospheric circulation in the recent surface melt increase over the Greenland ice sheet. *The Cryosphere*, **7**(1), 241-248, https://doi.org/10.5194/tc-7-241-2013

Francis, J.A., and S.J. Vavrus (2012). Evidence linking Arctic amplification to extreme weather in mid-latitudes. *Geophys. Res. Lett.*, **39**(6), L06801. https://doi.org/10.1029/2012GL051000

Gelaro, R., W. McCarty, M.J. Suárez, R. Todling, A. Molod, L. Takacs, C.A. Randles, A. Darmenov, M.G. Bosilovich, R. Reichle, K. Wargan, L. Coy, R. Cullather, C. Draper, S. Akella, V. Buchard, A. Conaty, A.M. da Silva, W. Gu, G. Kim, R. Koster, R. Lucchesi, D.

Merkova, J.E. Nielsen, G. Partyka, S. Pawson, W. Putman, M. Rienecker, S.D. Schubert, M. Sienkiewicz, and B. Zhao (2017). The Modern-Era Retrospective Analysis for Research and Applications, version 2 (MERRA-2). *J. Climate*, **30**(14), 5419-5454. https://doi.org/10.1175/JCLI-D-16-0758.1

Gillett, N.P., and J.C. Fyfe (2013). Annular mode changes in the CMIP5 simulations. *Geophys. Res. Lett.*, **40**(6), 1189-1193. https://doi.org/10.1002/grl.50249

GRACE-FO (2019). GRACE-FO Level-2 Monthly Geopotential Spherical Harmonics CSR Release 6.0 (RL06). Ver. 6. PO.DAAC, CA, USA. Dataset accessed 2019-11-25 at https://doi.org/10.5067/GFL20-MC060

Graeter, K.A., E.C. Osterberg, D.G. Ferris, R.L. Hawley, H.P. Marshall, G. Lewis, T. Meehan, F. McCarthy, T. Overly, and S.D. Birkel (2018). Ice core records of West Greenland melt and climate forcing. *Geophys. Res. Lett.*, **45**(7), 3164-3172. https://doi.org/10.1002/2017GL076641

Graham, E., and G. Huggett, Eds. (2019). New UK maximum air temperature record. *Weather*, **74**(9), 294. https://doi.org/10.1002/wea.3347

Hall, D.K., J.C. Comiso, N.E. DiGirolamo, C.A. Shuman, J.E. Box, and L.S. Koenig (2013). Variability in the surface temperature and melt extent of the Greenland ice sheet from MODIS. *Geophys. Res. Lett.*, **40**(10), 2114-2120. https://doi:10.1002/grl.50240

Hall, D.K., R.I. Cullather, N.E. DiGirolamo, J.C. Comiso, B.C. Medley, and S.M. Nowicki (2018). A multilayer surface temperature, surface albedo and water vapor product of Greenland from MODIS. *Remote Sens.*, **10**(4), 555. https://doi.org/10.3390/rs10040555

Häkkinen, S., D.K. Hall, C.A. Shuman, D.L. Worthen, and N.E. DiGirolamo (2014). Greenland ice sheet melt from MODIS and associated atmospheric variability. *Geophys. Res. Lett.*, **41**(5), 1600-1607. https://dx.doi.org/10.1002/2013GL059185

Hanna, E., P. Huybrechts, K. Steffen, J. Cappelen, R. Huff, C. Shuman, T. Irvine-Fynn, S. Wise, and M. Griffiths (2008). Increased runoff from melt from the Greenland Ice Sheet. A response to global warming. *J. Climate*, **21**(2), 331-341. https://dx.doi.org/10.1175/2007JCLI1964.1

Hanna, E., J.M. Jones, J. Cappelen, S.H. Mernild, L. Wood, K. Steffen, and P. Huybrechts (2013). The influence of North Atlantic atmospheric and oceanic forcing effects on 1900–2010 Greenland summer climate and ice melt/runoff. *Int. J. Climatol.*, **33**(4), 862-880. https://doi.org/10.1002/joc.3475

Hanna, E., X. Fettweis, S.H. Mernild, J. Cappelen, M.H. Ribergaard, C.A. Shuman, K. Steffen, L. Wood, and T.L. Mote (2014). Atmospheric and oceanic climate forcing of the exceptional Greenland ice sheet surface melt in summer 2012. *Int. J. Climatol.*, **34**(4), 1022-1037. https://doi.org/10.1002/joc.3743

Hanna, E., T.E. Cropper, P.D. Jones, A.A. Scaife, and R. Allan (2015), Recent seasonal asymmetric changes in the NAO (a marked summer decline and increased winter variability) and associated changes in the AO and Greenland Blocking Index. *Int. J. Climatol.*, **35**(9), 2540-2554. https://doi.org/10.1002/joc.4157

Hanna, E., T.E. Cropper, R.J. Hall, and J. Cappelen (2016). Greenland Blocking Index 1851–2015. A regional climate change signal. *Int. J. Climatol.*, **36**(15), 4847-4861. https://doi.org/10.1002/joc.4673

Hofer, S., A.J. Tedstone, X. Fettweis, and J.L. Bamber (2017). Decreasing cloud cover drives the recent mass loss on the Greenland Ice Sheet. *Science Advances*, **3**(6), e1700584. https://doi.org/10.1126/sciadv.1700584

The IMBIE Team (2019). Mass balance of the Greenland Ice Sheet from 1992 to 2018. *Nature*. https://doi.org/10.1038/s41586-019-1855-2

Lim, Y.-K., S.D. Schubert, S.M.J. Nowicki, J.N. Lee, A.M. Molod, R.I. Cullather, B. Zhao, and I. Velicogna (2016). Atmospheric summer teleconnections and Greenland Ice Sheet surface mass variations. Insights from MERRA-2. *Environ. Res. Lett.*, **11**(2), 024002. https://doi.org/10.1088/1748-9326/11/2/024002

Liu, C., and E.A. Barnes (2015). Extreme moisture transport into the Arctic linked to Rossby wave breaking. *J. Geophys. Res.*, **120**(9), 3774-3788. doi:10.1002/2014JD022796

Liu, J.P., Z.Q. Chen, J. Francis, M.R. Song, T. Mote, and Y.Y. Hu (2016). Has Arctic sea ice loss contributed to increased surface melting of the Greenland Ice Sheet? *J. Climate*, **29**(9), 3373-3386. https://doi.org/10.1175/JCLI-D-15-0391.1

Loomis, B.D., K.E. Rachlin, and S.B. Luthcke (2019). Improved Earth oblateness rate reveals increased ice sheet losses and mass-driven sea level rise. *Geophys. Res. Lett.*, **46**(12), 6910-6917. https://doi.org/10.1029/2019GL082929

Loomis, B.D., K.E. Rachlin, D.N. Wiese, F.W. Landerer, and S.B. Luthcke (2020). Replacing GRACE/GRACE-FO C30 with satellite laser ranging. Impacts on Antarctic Ice Sheet mass change. *Geophys. Res. Lett.*, **47**(3), e2019GL085488. https://doi.org/10.1029/2019GL085488

Magnusson, L. (2019). The 2019 western European heatwaves. ECMWF Newsletter, No. 161, pp. 2-3. Reading, United Kingdom: European Centre for Medium Range Weather Forecasts.

Mattingly, K.S., T.L. Mote, and X. Fettweis (2018). Atmospheric river impacts on Greenland Ice Sheet surface mass balance. *J. Geophys. Res.*, **123**(16), 8538-8560. https://doi.org/10.1029/2018JD028714

McGrath, D., W. Colgan, N. Bayou, A. Muto, and K. Steffen (2013). Recent warming at Summit, Greenland. Global context and implications. *Geophys. Res. Lett.*, **40**(10), 2091-2096, https://doi.org/10.1002/grl.50456.

Meredith, M., M. Sommerkorn, S. Cassotta, C. Derksen, A. Ekaykin, A. Hollowed, G. Kofinas, A. Mackintosh, J. Melbourne-Thomas, M.M.C. Muelbert, G. Ottersen, H. Pritchard, and E.A.G. Schuur (2019). Polar regions. In Pörtner, H.-O., D.C. Roberts, V. Masson-Delmotte, P. Zhai, M. Tignor, E. Poloczanska, K. Mintenbeck, A. Alegría, M. Nicolai, A. Okem, J. Petzold, B. Rama, N.M. Weyer (Eds.), *IPCC Special Report on the Ocean and Cryosphere in a Changing Climate* (pp. 203-320). Geneva, Switzerland: IPCC Intergovernmental Panel on Climate Change.

Mioduszewski, J.R., A.K. Rennermalm, A. Hammann, M. Tedesco, E.U. Noble, J.C. Stroeve, and T.L. Mote (2016). Atmospheric drivers of Greenland surface melt revealed by self-organizing maps. *J. Geophys. Res.*, **121**(D10), 5095-5114. https://doi.org/10.1002/2015JD024550

Moeller, C., R. Frey, E. Borbas, W.P. Menzel, T. Wilson, A. Wu, and X. Geng (2017). Improvements to Terra MODIS L1B, L2, and L3 science products through using crosstalk corrected L1B radiances. *Proc. SPIE 10402, Earth Observing Systems XXII*, 104020O. https://doi.org/10.1117/12.2274340

National Research Council (2014). *Linkages Between Arctic Warming and Mid-Latitude Weather Patterns: Summary of a Workshop*. The National Academies Press, Washington, D.C., 85 p. https://doi.org/10.17226/18727

Neff, W. (2018). Atmospheric rivers melt Greenland. *Nature Climate Change*, **8**(10), 857-858. https://doi.org/10.1038/s41558-018-0297-4

Neff, W., G.P. Compo, F.M. Ralph, and M.D. Shupe (2014). Continental heat anomalies and the extreme melting of the Greenland ice surface in 2012 and 1889. *J. Geophys. Res. Atmos.*, **119**(11), 6520-6536. https://doi.org/10.1002/2014JD021470

Nghiem, S. V., D.K. Hall, T.L. Mote, M. Tedesco, M.R. Albert, K. Keegan, C.A. Shuman, N.E. DiGirolamo, and G. Neumann (2012). The extreme melt across the Greenland ice sheet in 2012, *Geophys. Res. Lett.*, **39**(20), L20502. https://doi.org/10.1029/2012GL053611

Nienow, P.W., A.J. Sole, D.A. Slater, and T.R. Cowton (2017). Recent advances in our understanding of the role of meltwater in the Greenland Ice Sheet system. *Current Climate Change Rep.*, **3**, 330-344. https://doi.org/10.1007/s40641-017-0083-9

Noël, B., X. Fettweis, W.J. van de Berg, M.R. van den Broeke, and M. Erpicum (2014). Sensitivity of Greenland Ice Sheet surface mass balance to perturbations in sea surface temperature and sea ice cover. A study with the regional climate model MAR. *The Cryosphere*, **8**(5), 1871-1883. https://doi.org/10.5194/tc-8-1871-2014

Peltier, W.R., D.F. Argus, and R. Drummond (2018). Comment on "An Assessment of the ICE-6G_C (VM5a) Glacial Isostatic Adjustment Model" by Purcell et al. *J. Geophys. Res. Solid Earth*, **123**(2), 2019-2018. https://doi.org/10.1002/2016JB013844

478 Rajewicz, J., and S.J. Marshall (2014). Variability and trends in anticyclonic circulation over the
479 Greenland ice sheet, 1948–2013. *Geophys. Res. Lett.*, **41**(8), 2842-2850.
480 https://doi.org/10.1002/2014GL059255
481 Randles, C.A., A.M. da Silva, V. Buchard, A. Darmenov, P.R. Colarco, V. Aquila, H. Bian, E.P.
482 Nowottnick, X. Pan, A. Smirnov, H. Yu, and R. Govindaraju (2017). The MERRA-2 aerosol
483 assimilation. NASA Tech. Rep. NASA/TM-2016-104606/Vol. 45, 140 p.
484 Reeves Eyre, J.E., and X. Zeng (2017). Evaluation of Greenland near surface air temperature
485 datasets. *The Cryosphere,* **11**(4), 1591-1605. https://doi.org/10.5194/tc-11-1591-2017
486 Rennermalm, A.K., L.C. Smith, J.C. Stroeve, and V.W. Chu (2009). Does sea ice influence
487 Greenland ice sheet surface-melt? *Environ. Res. Lett.*, **4**(2), 024011.
488 https://doi.org/10.1088/1748-9326/4/2/024011
489 Smith, A., N. Lott, and R. Vose (2011). The Integrated Surface Database. Recent developments
490 and partnerships. *Bull. Amer. Meteorol. Soc.*, **92**(6), 704-708.
491 https://doi.org/10.1175/2011BAMS3015.1
492 Smith, L.C., K. Yang, L.H. Pitcher, B.T. Overstreet, V.W. Chu, Å.K. Rennermalm, J. Ryan,
493 M.G. Cooper, C.J. Gleason, M. Tedesco, J. Jeyaratnam, D. van As, M.R. van den Broeke,
494 W.J. van de Berg, B. Noël, P.L. Langen, R.I. Cullather, M.J. Willis, A. Hubbard, J.E. Box,
495 B.A. Jenner, and A.E. Behar (2017). Direct measurements of meltwater runoff on the
496 Greenland Ice Sheet surface. *Proc. Natl. Acad. Sci.*, **114**(50), E10622-E10631.
497 https://doi.org/10.1073/pnas.1707743114
498 Steffen, K., S.V. Nghiem, R. Huff, and G. Neumann (2004). The melt anomaly of 2002 on the
499 Greenland Ice Sheet from active and passive microwave satellite observations. *Geophys. Res.*
500 *Lett.*, **31**(20), L20402. https://doi.org/10.1029/2004GL020444

Stroeve, J.C., J.R. Mioduszewski, A. Rennermalm, L.N. Boisvert, M. Tedesco, and D. Robinson (2017). Investigating the local-scale influence of sea ice on Greenland surface melt. *The Cryosphere*, **11**(5), 2363-2381. https://doi.org/10.5194/tc-11-2363-2017

Sun, Y., R. Riva, and P. Ditmar (2016). Optimizing estimates of annual variations and trends in geocenter motion and J2 from a combination of GRACE data and geophysical models. *J. Geophys. Res. Solid Earth*, **121**(11), 8352-8370. https://doi.org/10.1002/2016JB013073

Swenson, S., and J. Wahr (2002). Methods for inferring regional surface-mass anomalies from Gravity Recovery and Climate Experiment (GRACE) measurements of time-variable gravity, *J. Geophys. Res.*, **107**(B9), 2193, https://doi.org/10.1029/2001JB000576

Tedesco, M., and X. Fettweis (2019). Unprecedented atmospheric conditions (1948 - 2019) drive the 2019 exceptional melting season over the Greenland ice sheet. *The Cryosphere Discuss*. https://doi.org/10.5194/tc-2019-254

Tedesco, M., M. Serreze, and X. Fettweis (2008). Diagnosing the extreme surface melt event over southwestern Greenland in 2007. *The Cryosphere*, **2**(2), 159-166. https://doi.org/10.5194/tc-2-159-2008

Tedesco, M., X. Fettweis, M.R. van den Broeke, R.S.W. van de Wal, C.J.P.P. Smeets, W.J. van de Berg, M.C. Serreze, and J.E. Box (2011). The role of albedo and accumulation in the 2010 melting record in Greenland. *Environ. Res. Lett.*, **6**(1), 014005. https://doi.org/10.1088/1748-9326/6/1/014005

Tedesco, M., X. Fettweis, T. Mote, J. Wahr, P. Alexander, J.E. Box, and B. Wouters (2013). Evidence and analysis of 2012 Greenland records from spaceborne observations, a regional climate model and reanalysis data. *The Cryosphere*, **7**(2), 615-630. https://doi.org/10.5194/tc-7-615-2013

524 Tedesco, M., T. Mote, X. Fettweis, E. Hanna, J. Jeyaratnam, J.F. Booth, R. Datta, and K. Briggs
525 (2016). Arctic cut-off high drives the poleward shift of a new Greenland melting record.
526 *Nature Comm.*, **7**, 11723. https://doi.org/10.1038/ncomms11723
527 Thomas, J. L., C.M. Polashenski, A.J. Soja, L. Marelle, K.A. Casey, H.D. Choi, J.-C. Raut, C.
528 Wiedinmyer, L.K. Emmons, J.D. Fast, J. Pelon, K.S. Law, M.G. Flanner, and J.E. Dibb
529 (2017). Quantifying black carbon deposition over the Greenland ice sheet from forest fires in
530 Canada. *Geophys. Res. Lett.*, **44**(15), 7965-7974. https://doi.org/10.1002/2017GL073701.
531 Trigo, R.M., M.A. Valente, I.F. Trigo, P.M.A. Miranda, A.M. Ramos, D. Paredes, and R. García-
532 Herrera (2008). The impact of North Atlantic wind and cyclone trends on European
533 precipitation and significant wave height in the Atlantic. *Annals New York Acad. Sci.*,
534 **1146**(1), 212-234. https://doi.org/10.1196/annals.1446.014
535 Trusel, L.D., S.B. Das, M.B. Osman, M.J. Evans, B.E. Smith, X. Fettweis, J.R. McConnell,
536 B.P.Y. Noël, and M.R. van den Broeke (2018). Nonlinear rise in Greenland runoff in response
537 to post-industrial Arctic warming. *Nature*, **564**(7734), 104-108.
538 https://doi.org/10.1038/s41586-018-0752-4
539 van den Broeke, M.R., J. Box, X. Fettweis, E. Hanna, B. Noël, M. Tedesco, D. van As, W.J. van
540 de Berg, and L. van Kampenhout (2017). Greenland Ice Sheet surface mass loss. Recent
541 developments in observation and modeling. *Curr. Clim. Change Rep.*, **3**(4), 345-356.
542 https://doi.org/10.1007/s40641-017-0084-8
543 van Tricht, K., S. Lhermitte, J.T.M. Lenaerts, I.V. Gorodetskaya, T.S. L'Ecuyer, B. Noël, M.R.
544 van den Broeke, D.D. Turner, and N.P.M. van Lipzig (2016). Clouds enhance Greenland ice
545 sheet meltwater runoff. *Nature Comm.*, **7**, 10266. https://doi.org/10.1038/ncomms10266

546 Wang, W., C.S. Zender, D. van As, and N.B. Miller (2019). Spatial distribution of melt season
547 cloud radiative effects over Greenland. Evaluating satellite observations, reanalyses, and
548 model simulations against in situ measurements. *J. Geophys. Res.*, **124**(1), 57-71.
549 https://doi.org/10.1029/2018JD028919
550 Zwally, H.J., M.B. Giovinetto, M.A. Beckley, and J.L. Saba (2012). *Data from: Antarctic and*
551 *Greenland Drainage Systems*. NASA GSFC Cryospheric Sciences Laboratory. Available
552 online at: http://icesat4.gsfc.nasa.gov/cryo_data/ant_grn_drainage_systems.php
553

List of Figures

1. (a) The contour line corresponding to a stream function value of $-5 \cdot 10^7$ m^2 s computed from MERRA-2 250 hPa winds, for successive 12-hr instances from 20-July through 2-August 2019. The projection highlights zonal and meridional departures. GrIS drainage basins from Zwally et al. (2012) are labelled. A domain used for pattern correlation is indicated with a green dashed line, see text. (b) As in (a) but for melt events (Box et al., 2010; Nghiem et al., 2012) ending 12-June 2007, 21-July 2010, and 12-July 2012. (c, d, e) 700 hPa temperature field for selected times in 2019, shaded every 0.1°C. Grey shading indicates no data (intersection of 700 hPa level and the surface). The 500 hPa geopotential height field is indicated with contour lines every 20 m. The 250 hPa wind field is indicated with vectors. The reference magnitude is 20 m s^{-1}.
2. The extent of GrIS surface melt over the three-day period 29-July to 31-July 2019 from (a) MODIS retrieved skin temperature, and (b) MERRA-2. Stars indicate the location of meteorological stations Scoresbysund (Ittoqqortoormiit, 71°N, 22°W), Danmarkshavn (77°N, 19°W), and Summit (73°N, 39°W). Temperature sounding profiles are indicated for these stations (c, d, e) over the period 23-July to 03-August. Hourly surface air temperature time series are shown over the period of the melt event (f).
3. Surface energy budget components from (a) MERRA-2, averaged over GrIS basin 3, and (b) PROMICE AWS station SCO-U (72°N, 27°W, 970 m). Vertical bars indicate the spatial standard deviation of MERRA-2 over basin 3. Flux values are plotted in W m^{-2}, and air temperature is plotted in °C.
4. Annual cycle of GRACE/GRACE-FO derived mass anomaly relative to each year's maximum value for (a) total GrIS, (b) northern GrIS (Zwally basin 1), (c) eastern GrIS (Zwally basins 2

and 3), and (d) southern GrIS (Zwally basins 4, 5, and 6), in Gt. Select years are indicated, while dotted lines denote all other years in the GRACE/GRACE-FO record. Accumulated errors are shown for 2019; errors for all other years are considered in the analysis but are not overlaid here for clarity. The time series are plotted as anomalies relative to each year's maximum value, which generally occurs in winter and early spring for each of the basins shown.

Figure 1.

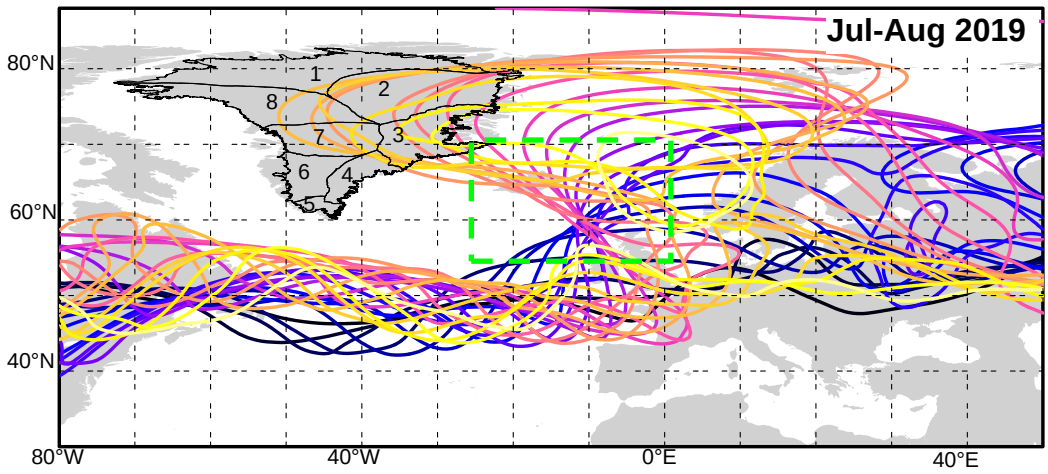
Jul-Aug 2019
80°N
60°N
40°N
80°W
40°W
0°E
40°E
1
2
3
4
5
6
7
8
21-Jul
22-Jul
23-Jul
24-Jul
25-Jul
26-Jul
27-Jul
28-Jul
29-Jul
30-Jul
31-Jul
1-Aug
2-Aug

(a)

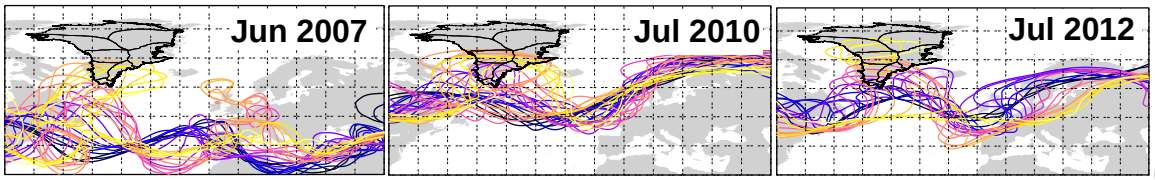
Jun 2007
Jul 2010
Jul 2012

(b)

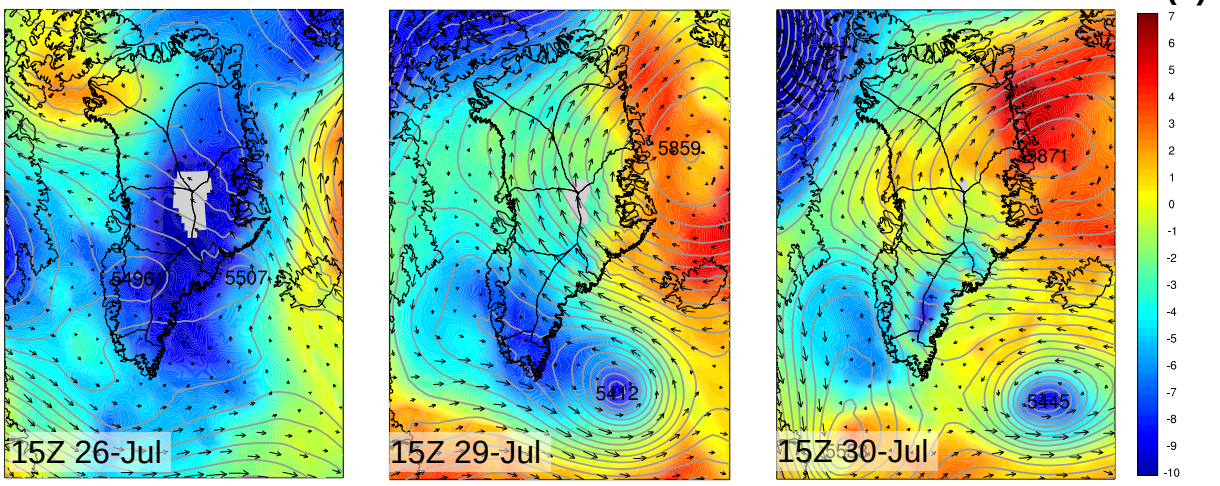
5496
5507
15Z 26-Jul
5859
5412
15Z 29-Jul
5871
5445
15Z 30-Jul
7
6
5
4
3
2
1
0
-1
-2
-3
-4
-5
-6
-7
-8
-9
-10

(c) (d) (e)

Figure 2.

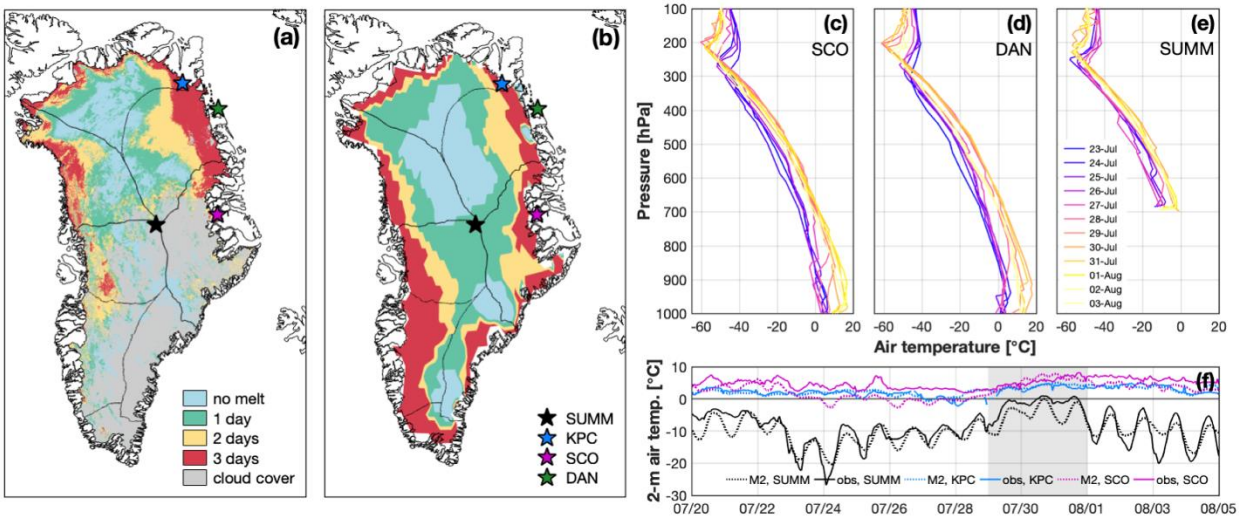
(a)
no melt
1 day
2 days
3 days
cloud cover
(b)
SUMM
KPC
SCO
DAN
(c)
SCO
(d)
DAN
(e)
SUMM
Pressure [hPa]
Air temperature [°C]
23-Jul
24-Jul
25-Jul
26-Jul
27-Jul
28-Jul
29-Jul
30-Jul
31-Jul
01-Aug
02-Aug
03-Aug
(f)
2-m air temp. [°C]
M2, SUMM
obs, SUMM
M2, KPC
obs, KPC
M2, SCO
obs, SCO
07/20
07/22
07/24
07/26
07/28
07/30
08/01
08/03
08/05

Figure 3.

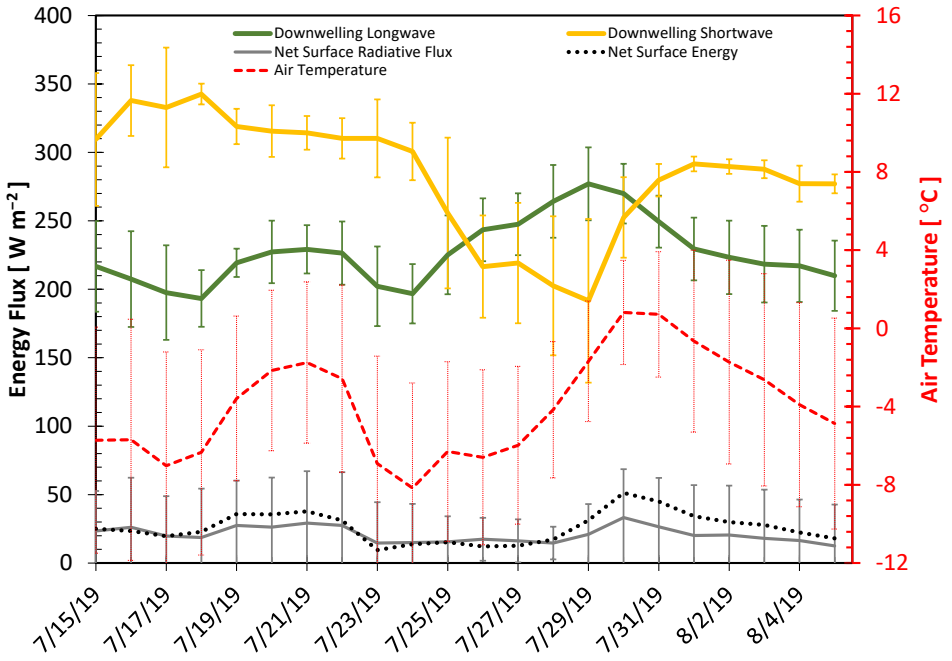
Downwelling Longwave
Downwelling Shortwave
Net Surface Radiative Flux
Net Surface Energy
Air Temperature
Energy Flux [W m⁻²]
Air Temperature [°C]
400
350
300
250
200
150
100
50
0
16
12
8
4
0
-4
-8
-12
7/15/19
7/17/19
7/19/19
7/21/19
7/23/19
7/25/19
7/27/19
7/29/19
7/31/19
8/2/19
8/4/19

(a)

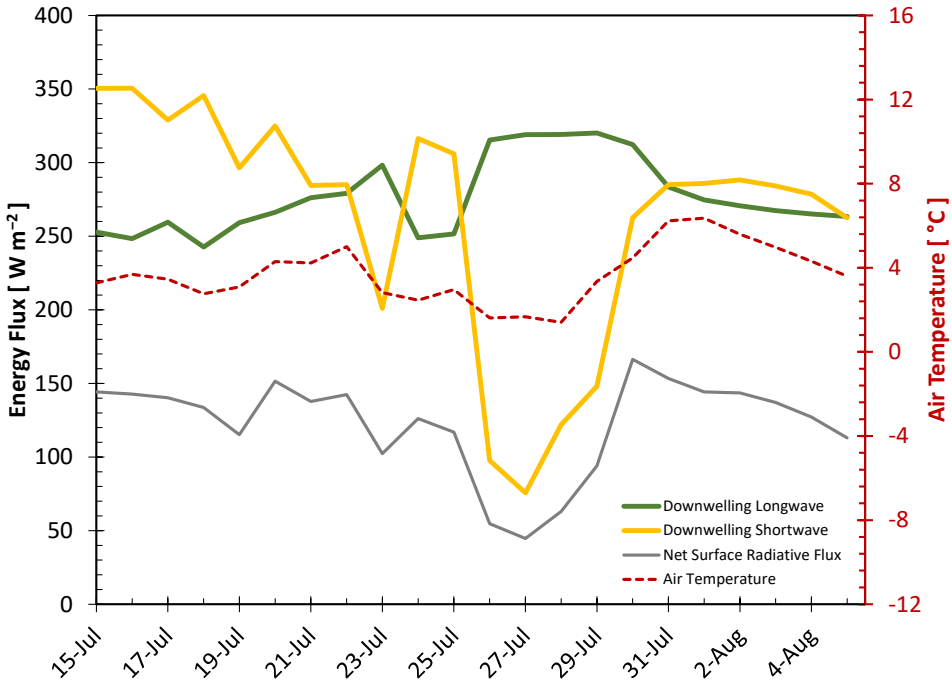
Energy Flux [W m⁻²]
Air Temperature [°C]
400
350
300
250
200
150
100
50
0
16
12
8
4
0
-4
-8
-12
Downwelling Longwave
Downwelling Shortwave
Net Surface Radiative Flux
Air Temperature
15-Jul
17-Jul
19-Jul
21-Jul
23-Jul
25-Jul
27-Jul
29-Jul
31-Jul
2-Aug
4-Aug

(b)

Figure 4.

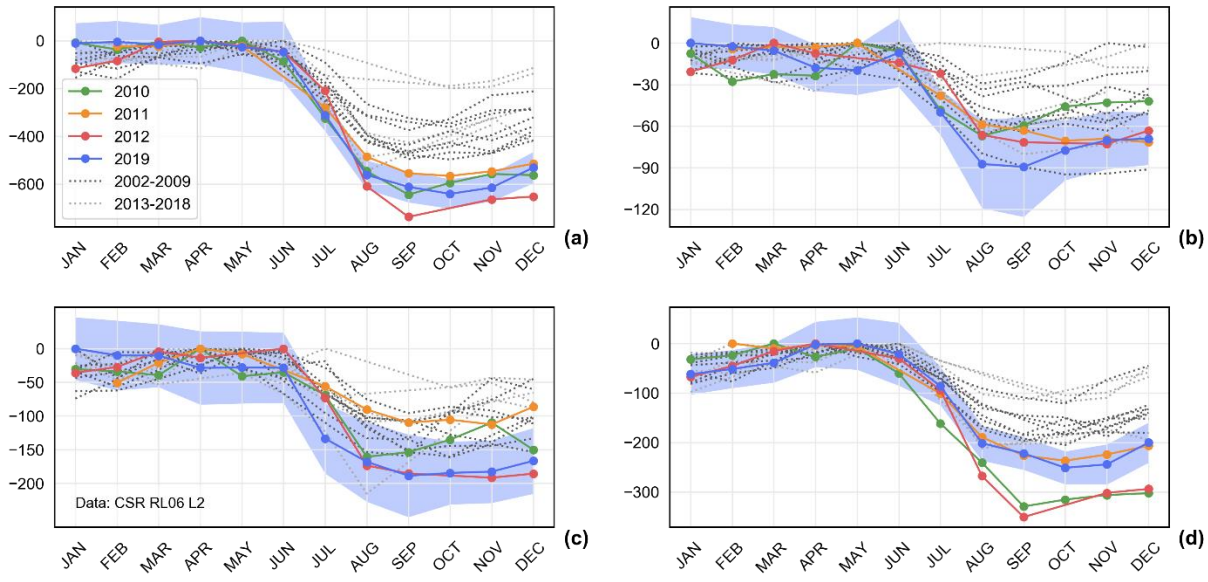
0
−200
−400
−600
2010
2011
2012
2019
2002-2009
2013-2018
JAN
FEB
MAR
APR
MAY
JUN
JUL
AUG
SEP
OCT
NOV
DEC
(a)
0
−30
−60
−90
−120
(b)
0
−50
−100
−150
−200
Data: CSR RL06 L2
(c)
0
−100
−200
−300
(d)